IOP Publishing
Plasma Sources Science and Technology
Plasma Sources Sci. Technol. **27** (2018) 015016 (14pp)
https://doi.org/10.1088/1361-6595/aaa5da

Interaction of positive streamers in air with bubbles floating on liquid surfaces: conductive and dielectric bubbles

Natalia Yu Babaeva[1,3], **George V Naidis**[1] **and Mark J Kushner**[2]

[1] Joint Institute for High Temperatures, Russian Academy of Sciences, Moscow 125412, Russia
[2] Department of Electrical Engineering and Computer Science, University of Michigan, 1301 Beal Ave, Ann Arbor, MI 48109-2122 United States of America

E-mail: nybabaeva@gmail.com

Received 3 October 2017, revised 14 December 2017
Accepted for publication 8 January 2018
Published 25 January 2018

Abstract

The interaction of plasmas sustained in humid air with liquids produces reactive species in both the gas phase and liquid for applications ranging from medicine to agriculture. In several experiments, enhanced liquid reactivity has been produced when the liquid is a foam or a bubble coated liquid. To investigate the phenomena of streamers interacting with bubbles a two-dimensional computational investigation has been performed of streamer initiation and propagation on and inside hemispherical bubble-shells floating on a liquid surface. Following prior experiments, water and oil bubble-shells with an electrode located outside and inside the bubble were investigated. We found that positive air streamers interact differently with conductive water and dielectric oil bubbles. The streamer propagates along the external surface of a water bubble while not penetrating through the bubble due to screening of the electric field by the conducting shell. If the electrode is inserted inside the bubble, the path of the streamer depends on how deeply the electrode penetrates. For shallow penetration, the streamer propagates along the inner surface of the bubble. Due to the low conductivity of oil bubble-shells, the electric field from an external electrode penetrates into the interior of the bubble. The streamer can then be re-initiated inside the bubble.

Keywords: conductive and dielectric bubbles, water and oil bubble-shells, streamers interacting with bubbles

1. Introduction

Plasma interacting with liquids comes in at least three varieties [1–3]. The first is a plasma sustained in the gas above the liquid, with or without contact of the active plasma with the liquid. Activation of the liquid largely occurs by solvation of gas phase radicals and ions through the liquid interface, though photolysis and direct charge exchange with the liquid also occur. The second method is production of a gas phase plasma inside submerged bubbles within the liquid. The liquid activation process is largely the same as the external plasma. The third is direct production of an electric discharge in the liquid. Although there are instances where these in-liquid discharges are produced in the absence of bubbles [4], the majority of discharges in liquids are likely accelerated by bubbles, pre-existing or self-generated. As such, the majority of applications of plasmas in liquids are based on plasma production inside gas bubbles [5–10]. To selectively activate the liquid, plasmas are often sustained in bubbles filled with different gases and artificially injected into liquids [11–13]. The efficiency of transfer of gas phase plasma produced reactivity into liquids by liquid-hugging plasmas or plasmas in bubbles has motivated research into several configurations of plasma-liquid systems [14–18]. Several roadmaps and reviews have recently assessed key research challenges in these areas [19–22].

From a classical perspective, foams are gas dispersions in liquids. They are comprised of a myriad of small bubbles of

[3] Author to whom any correspondence should be addressed.

mechanical or chemical origin. The bubbles are separated by thin films of a liquid [23]. Gas typically constitutes the largest volume fraction of a foam. Plasmas interacting with foams and bubble-covered liquids have attracted interest as means to rapidly activate liquids. Activation of liquid using gas phase plasmas is ultimately transport limited. The large surface-to-volume ratio of the liquid shells of bubbles provides a means to accelerate activation of the liquid, in some cases having plasma on both sides of the shell. For example, recent experiments [24] showed that the plasma-foam system is one of the most efficient methods for hydrogen peroxide production in a liquid phase.

In many applications, foams are not desired, and so processes are used to disperse or *break* the foam [25]. The most commonly used methods for foam destruction are the addition of chemical antifoam reagents which may have significant unwanted side effects [25], and mechanical foam breaking based on subjecting the foams to shear stress with an abrupt pressure drop which results in bursting the bubble [26, 27]. Physical methods for foam control include electrical *foam breakers* based on interacting an electric discharge with the foamy region to break up the foam leading to a decrease in the volume of the foam. Large bubbles can create numerous small bubbles when they rupture, rather than vanishing [28]. A preliminary study on the control of water foam by pulsed high voltage discharges achieved favorable results using foams with thickness of 10 μm [29]. This process involved passing bubbles through the gap between the two horizontally fixed stainless steel mesh electrodes above the water surface [30]. The air in the bubbles was released thus decreasing the growth speed of the foam. The bursting of the bubble was attributed to the streamers of the discharge penetrating through the surface of the bubbles.

In plasma-foam systems the electric current of the discharge simultaneously interacts with a large number of bubbles, often having different sizes, a condition which complicates understanding the fundamental physics of the process. One promising approach to investigate the fundamentals of plasma-foam interactions was introduced by Akishev *et al* [31] who simplified the problem to experimentally investigating a single streamer in air interacting with a single large bubble floating on liquid. The single-filament streamer discharge originated from a fixed point electrode located above or inside the bubble. The experiments showed that in many cases streamers striking a bubble resulted in its destruction and that large bubbles (with a base diameter >5 mm) were more susceptible to streamer initiated destruction than small bubbles (<2–3 mm). The experiments addressed both water bubble-shells floating on tap water and oil bubble-shells floating on oil. The streamers interacted differently with the conductive water bubble compared to the dielectric oil bubble. For example, a positive streamer in humid air initiated outside a water bubble-shell propagates along the external surface of the bubble as a surface ionization wave (SIW). A streamer striking an oil bubble gives the appearances of penetrating through the bubble into the interior, likely a result of the streamer being reinitiated inside the bubble.

In this paper, results from a computational investigation of streamers sustained in humid air intersecting with bubble-shells are presented, aligning with experiments performed by Akishev *et al* [31]. The goal of this study is to provide insights into the mechanisms whereby streamers interact with liquid bubble-shells, as the first step towards understanding how such plasmas interacting with foams potentially provide a more efficient method to activate the liquid. All computations were performed for positive streamers propagating in humid air intersecting bubble-shells also filled with humid air. In agreement with the experiments, we found that for conductive bubble-shells akin to tap water, a streamer launched from an electrode outside the bubble, when striking the bubble, will propagate over the outside surface of the bubble as a SIW. If the electrode is placed inside the water bubble with the tip near the inner surface, the streamer propagates over the inner surface of the bubble. If the electrode tip is placed deeply inside the bubble, the streamer will propagate directly towards ground. For otherwise the same conditions but for a non-conductive bubble-shell, the electric field penetrates inside the bubble to a greater degree than the more conductive water shell. As such, the streamer can be reinitiated inside the bubble-shell if there is finite preionization. We also show that the charge accumulated on both sides of the bubbles as a result of the SIW depends on the bubble conductivity. For a non-conductive oil bubble, these charges may produce forces large enough to rupture the bubble on a longer time scale.

The model, geometry and reaction mechanism are discussed in section 2. Evolution of a streamer interacting with a water bubble-shell with the powered electrode outside and inside the bubble is discussed in section 3. In section 4, we discuss the consequences of the streamer interaction and re-initiation with oil bubble-shell. Concluding remarks are in section 5.

2. Description of the model

The model used in this investigation, nonPDPSIM, is a modular, two-dimensional fluid hydrodynamics simulation. The modules in this model are sequentially executed while simultaneously solving Poisson's equation for the electric potential and transport equations for charged and neutral species. Poisson's equation is solved throughout the computational domain, including the gas phase, and liquid and solid materials. The electron temperature, T_e, is obtained by solving an electron energy conservation equation with transport and rate coefficients provided by solutions of Boltzmann's equation. Photoionization is also included which accounts for the production of precursor electrons ahead of the streamer front. A detailed description of the nonPDPSIM modeling platform can be found in [32, 33].

The gas mixture is atmospheric pressure humid air $N_2/O_2/H_2O = 79.5/19.5/1$ at 300 K. There are 24 species included in the model and 175 reactions between them. The

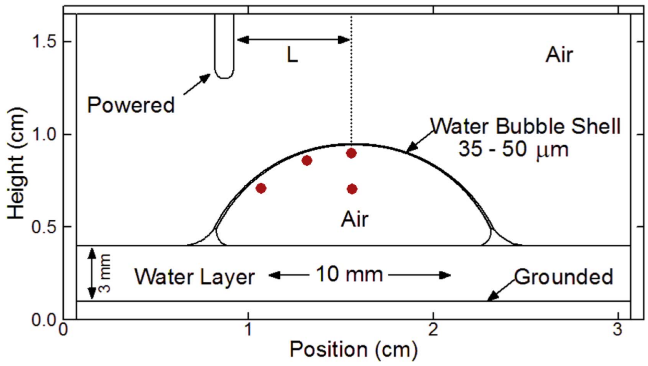

Figure 1. The total computational domain representing the experiments of Akishev *et al* [31]. Bubbles in humid air and filled with ambient air composed of water or oil 35–50 μm thick float on a 3 mm layer of water or oil. The diameter of the bubble base is 15 mm. The gap between the electrode and the liquid surface is 9 mm, applied voltage is 25 kV. The pin electrode is displaced a distance L (1–10 mm) from the axis. The red dots show the different locations of the initial seed charges that were investigated.

species included in the model are: N_2, $N_2(v)$, N_2^*, N_2^{**}, N_2^+, N, N^*, N^+, N_4^+, O_2, O_2^*, O_2^+, O_2^-, O^-, O, O^*, O^+, O_3, H_2O, H_2O^+, H_2, H, OH and electrons. The reaction mechanism is identical to that used in [34]. Since the timescale of interest is that of the streamer propagation and interaction with the bubble, less than tens of ns, cluster ions and higher order species (such as nitrogen oxides) have not been included in the reaction mechanism for computational expediency as these species typically form on longer timescales. We acknowledge that for repetitive pulsing, these species may have been formed on prior pulses and so may be present during the streamer propagation. Based on past experience, the dynamics of the ionization waves are weak functions of small concentrations of these species. Neutral transport was represented only by diffusion (no advective motion) and gas heating was not considered. By examining only the first tens of ns of streamer propagation in stagnant ambient gas, there would not be time for pressure gradients to initiate advective motion.

The total computational domain is shown in figure 1. This geometry is intended to represent the conditions and dimensions of the experiments performed by Akishev *et al* [31]. A liquid layer 3 mm thick is on the planar electrode. The bottom surface of the computational domain under the liquid representing the planar electrode is electrically grounded. The applied voltage is the potential boundary condition used for the pin electrode and on the top boundary. The derivative of the electric potential is set to zero on the left-and-right boundaries. Such boundary conditions provide stability to the numerical solution, while at the same not significantly affecting the dynamics of the plasma in the regions of high electric field that produce ionization.

Bubbles filled with ambient humid air are composed of a water or oil shell 35–50 μm thick on top of the liquid of the same composition. In the water case, both the shell and the underlying liquid are water. In the oil case, both the shell and the underlying liquid are oil. The diameter of the base of the bubble is 15 mm. The gap between the electrode and the liquid surface is 9 mm. The distance between the pin electrode and the top of a bubble along the central axis is 4 mm. The distance L between the electrode and the top of a bubble was varied from 1 to 10 mm. In order to investigate asymmetric geometries with the electrode displaced from the central axis, the calculations were done in planar, Cartesian coordinates.

An unstructured numerical mesh was used having triangular elements with different refinement regions to resolve the bubble-shell, bubble interior and the region near the high voltage electrode. The mesh consists of approximately 15 200 nodes, of which more than 9500 are in the plasma region to resolve the plasma filaments. The mesh spacing spanned from 4 μm in the path of the streamer (both in the gas phase and along the surface) to as large as 500 μm in the periphery of the mesh. The electrical potential is specified on the ground plane beneath the liquid and on the powered electrode. On non-metal points on the right and left boundaries of the computational mesh, von Neumann conditions are imposed, where the gradient of the electric potential, the electric field, is zero.

The water shell and water layer are treated as lossy dielectrics, and have relative permittivity $\varepsilon/\varepsilon_0 = 80$ and conductivity $\sigma = 7.5 \times 10^{-4}\,\Omega^{-1}\,\text{cm}^{-1}$, akin to tap water. The oil shell and oil layer have a relative permittivity of $\varepsilon/\varepsilon_0 = 2$ and a conductivity $\sigma = 1.5 \times 10^{-7}\,\Omega^{-1}\,\text{cm}^{-1}$. These values of conductivity are chosen to represent the experimental conditions [31]. The applied voltage (25 kV) is higher than in the experiment (15.2 kV) because we use a smooth rounded electrode to avoid numerical instability (near the powered electrode) as opposed to a sharpened tip electrode as used in experiment [31]. The voltage rise time is 0.1 ns, intended to represent a step-function in voltage. In most cases, to initiate the discharge, a small cloud of electrically neutral seed-charges (electrons and N_2^+) with a radius of 100 μm and a peak density of $1 \times 10^8\,\text{cm}^{-3}$ was placed near the tip of the powered electrode. The same cloud of seed-charges was placed inside the bubbles on the bubble axis to study the possible re-initiation of a streamer beneath the bubble-shell. To assess the sensitivity of predictions of the model to the position of the initial small cloud of plasma, clouds were placed at different locations shown by the red dots in figure 1. The initial plasma density was also uniformly set to $5 \times 10^3\,\text{cm}^{-3}$ inside the bubble. In general, the resulting behavior of the discharge was qualitatively the same to the base case except for a change in the time for development of the discharge. This latter observation is a result of the well-known *formative lag time* in breakdown where discharges take longer to develop as the initial electron density decreases [35].

The authors acknowledge that this problem is intrinsically three-dimensional in nature whereas the computational tool is two-dimensional. When the pin electrode is aligned with the central axis, a 2D simulation using cylindrical coordinates would be more rigorous. However, using Cartesian coordinates in 2D for all cases enables side-by-side comparisons of cases that may not have this symmetry, for example, when the pin-electrode is displaced from the axis. One direct consequence of using the 2D Cartesian coordinate system is that geometrical electric field enhancement (e.g. at

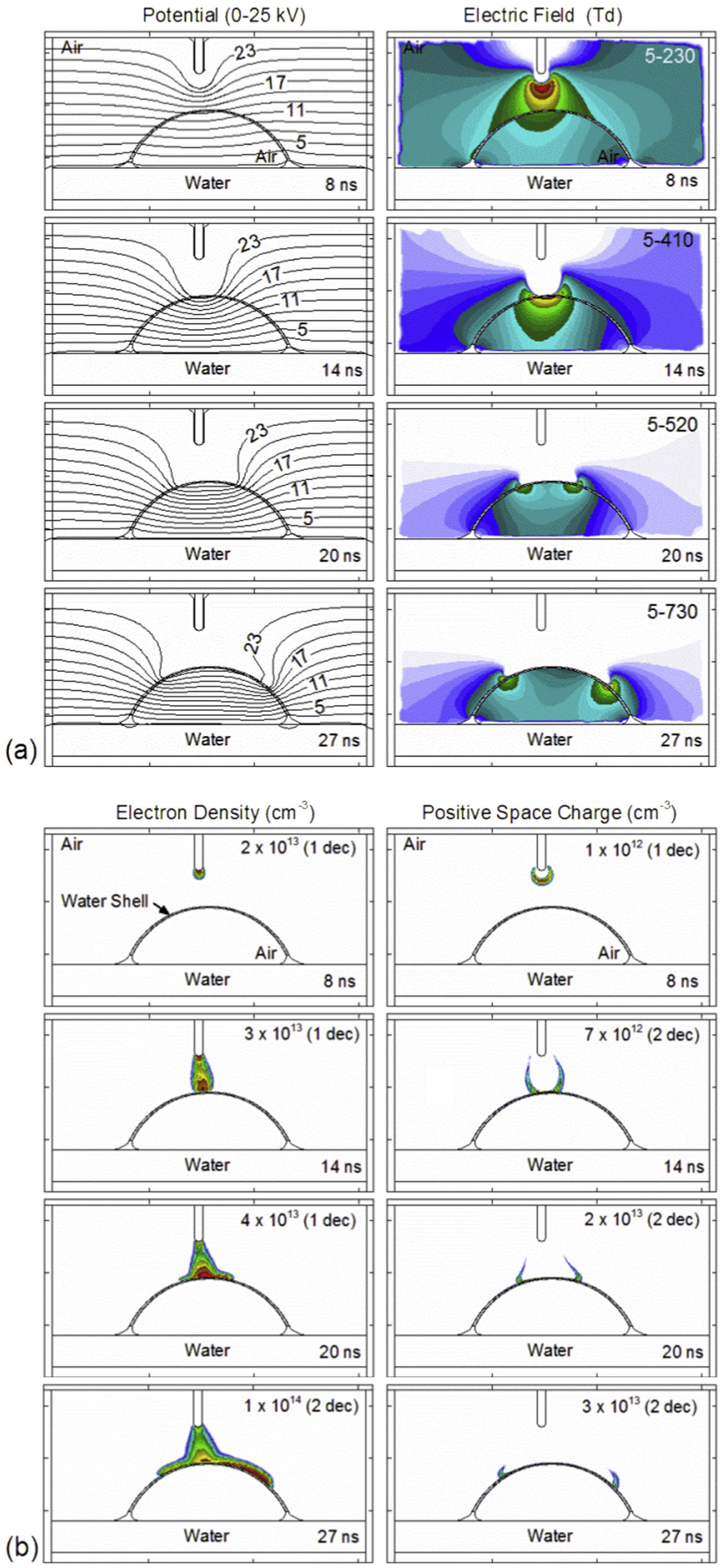

Figure 2. Time evolution of (a) plasma potential and electric field, and (b) electron density and positive space charge for a streamer interacting with a water bubble-shell with $L = 1$ mm. Potential lines are drawn every 2 kV. There is an enhancement of the electric field at the water shell-air boundary. The streamer approaches the surface of the bubble and spreads over it but does not penetrate into the bubble. The maximum value or range of values is shown for each frame.

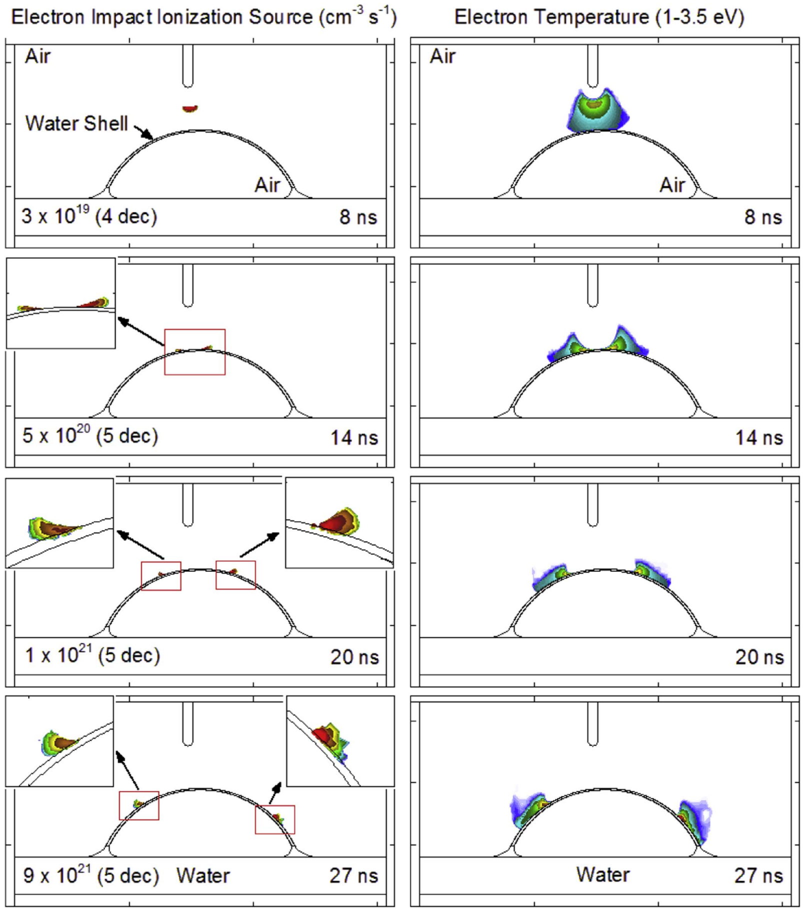

Figure 3. Time evolution of the electron impact ionization source and electron temperature for a water bubble-shell with $L = 1$ mm. There is non-zero electron temperature inside the bubble due to the present of a small amount of electrons. The insets show enlargements of the surface ionization wave. The maximum value or range of values is shown for each frame.

the tip of the electrode) is smaller than when fully resolved in 3D. It is for this reason that we use a higher value of potential than in the experiment.

3. Streamer interaction with a water bubble-shell

As the base case, we consider a positive streamer interacting with a water bubble-shell with the powered electrode having a 1 mm offset from the axis of the bubble ($L = 1$ mm). The time evolution of the electric potential and electric field as the streamer propagates from the pin electrode towards ground is shown in figure 2(a). (The potential lines are drawn every 2 kV.) The electron density and positive space charge are shown in figure 2(b), and the electron impact ionization source and electron temperature are shown in figure 3. The combined conductivity and dielectric constant of tap-water produces a capacitive material with resistive losses—that is, a lossy dielectric. The water has a dielectric relaxation time of $\tau = \varepsilon/\sigma = 9.4$ ns. The streamer propagates across the gap between the electrode and the surface of the bubble in about 10–13 ns, and its interaction with the bubble extends to about 27 ns. The shell of the bubble will both support some amount of charging while also shielding some of the applied potential from the interior of the bubble due to the dielectric relaxation time being commensurate with the total interaction time.

The electron density is 3×10^{13} cm^{-3} in the volume of the streamer, increasing to 10^{14} cm^{-3} when streamer touches the water shell. The trajectory of the streamer is not strictly vertical. As the streamer approaches the bubble it reorients to being nearly parallel to the surface normal of the bubble in recognition of the conductive properties of the bubble. (The electric field at the surface of a conductor is normal to the surface.) As the streamer approaches the bubble, the potential lines do penetrate through the shell and into the bubble, a consequence of the dielectric properties and thin dimension of the shell. This penetration of the electric field into the shell enables enhancement in the electric field at the surface of the bubble resulting from the refraction of potential lines at the bubble-shell boundary.

After striking the bubble, the volume streamer transforms into a surface streamer or SIW which then propagates over the bubble surface towards ground in both directions. There is almost no visible motion of the streamer from 14 to 20 ns, which results from the charging of the high capacitance of the water bubble-shell. (The local capacitance is $\approx$0.15 pF cm^{-2}.) The dielectric properties of the shell enable there to be positive charging to 3×10^{13} cm^{-3} at the surface which produces parallel components of the electric field which

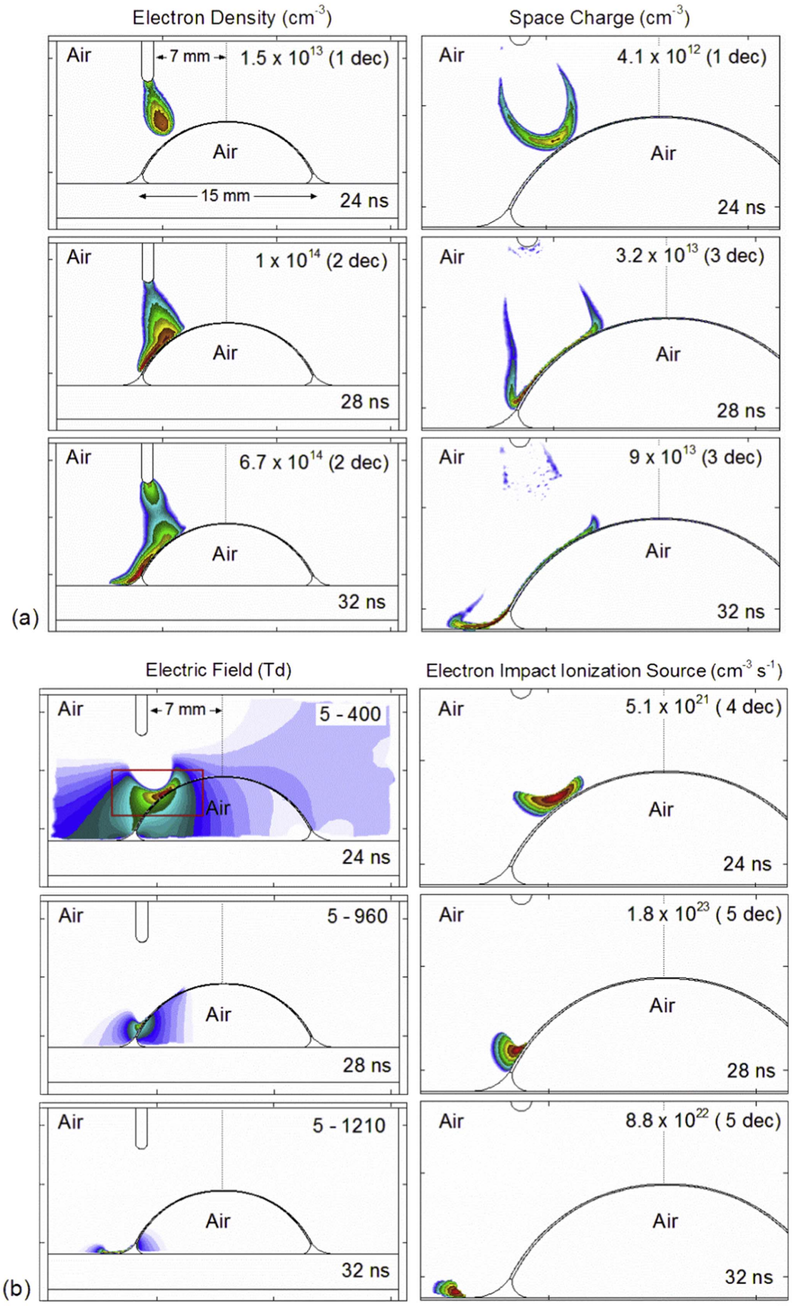

Figure 4. Streamer properties approaching and intersecting a water bubble-shell with $L = 7$ mm. (a) Electron density and positive charge and (b) electric field and electron impact ionization source. The maximum value or range of values is shown for each frame or set of frames. Magnification of the region within the red box is shown in figure 7(a).

initiate and then sustain the SIW. The electric field in the head of the volume streamer is 230 Td (1 Td $= 10^{-17}$ V cm^2) largely perpendicular to the surface. As the streamer propagates over the surface at 1.5×10^8 cm s^{-1}, compared to a propagation speed of 0.4×10^8 cm s^{-1} in crossing the gap, the electric field increases up to 520–730 Td largely parallel to the surface. These high values are typical for a surface streamer, producing a maximum in the electron impact ionization source of to 9×10^{21} cm^{-3} s^{-1} and electron temperature of 3.5 eV. In spite of the tip of the electrode being off-axis, the SIW propagates in both directions—*downhill* (towards the left) where the electric field parallel to the surface is enhanced by the applied vacuum electric field, and *uphill* (towards the right) where the electric field parallel to the surface is diminished by the applied electric field, but still sufficient to sustain the SIW.

The charging of the top surface of the bubble and the screening of the field by the conductive water-shell results in a maximum in electric field inside the bubble of 90 Td, which follows the peak in surface charging as the SIW propagates along the top surface. In spite of a preionization density of 1×10^8 cm^{-3} inside the bubble and this penetrating electric field, there is no avalanche nor streamer propagation inside the bubble. The combination of the finite conductivity of the

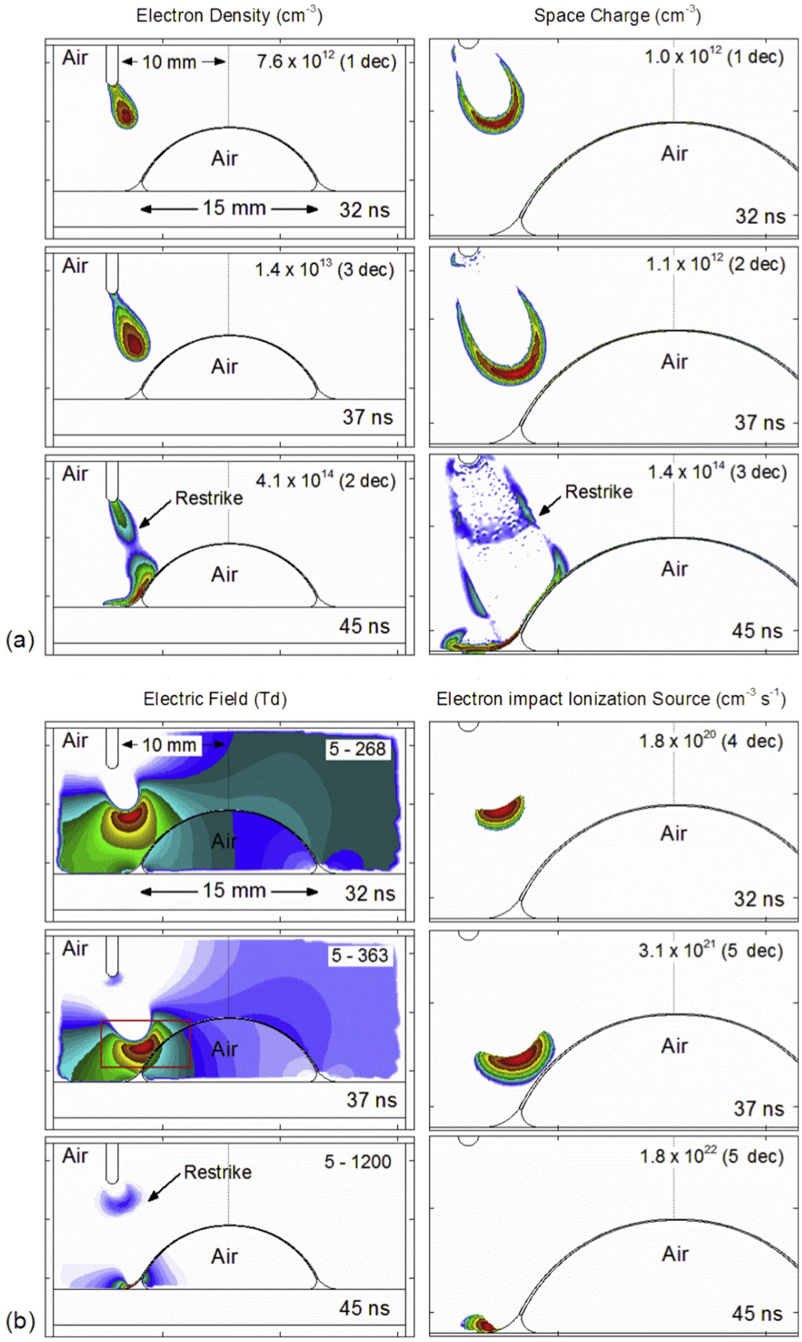

Figure 5. Streamer properties approaching and intersecting a water bubble-shell with $L = 10$ mm. (a) Electron density and positive charge; and (b) electric field and electron impact ionization source. The maximum value or range of values is shown for each frame or set of frames. Magnification of the region within the red box is shown in figure 7(b).

water shell and the charging of the surface, produce sufficient shielding to prevent avalanche inside the bubble.

Exhaustive studies have not been performed on the size of the computational domain and the location of boundaries on the streamer properties. However, we have confirmed that the width of the domain used in this investigation does not significantly affect the value of the electric field where avalanches occur—beginning at the tip of the electrode and at the head of the volume and SIW (see, for example, figure 2(a)).

Streamer properties (electron density, space charge, electric field and electron impact ionization source) with the point electrode offset from the axis are shown in figure 4 for $L = 7$ and figure 5 for $L = 10$ mm. The general trends are similar as those for $L = 1$ mm. However, since the effective gas-gap length is larger as L increases, the effective electric field is smaller for $L = 7$ and 10 mm compared to $L = 1$ mm. The progressively increasing curvature of the surface under the electrode tip as L increases then increasingly aligns the applied electric field with being parallel to the surface. As L increases, the vacuum electric fields begin to resemble those of the traditional point-to-plane geometry, with the electric field progressively directed towards the ground plane.

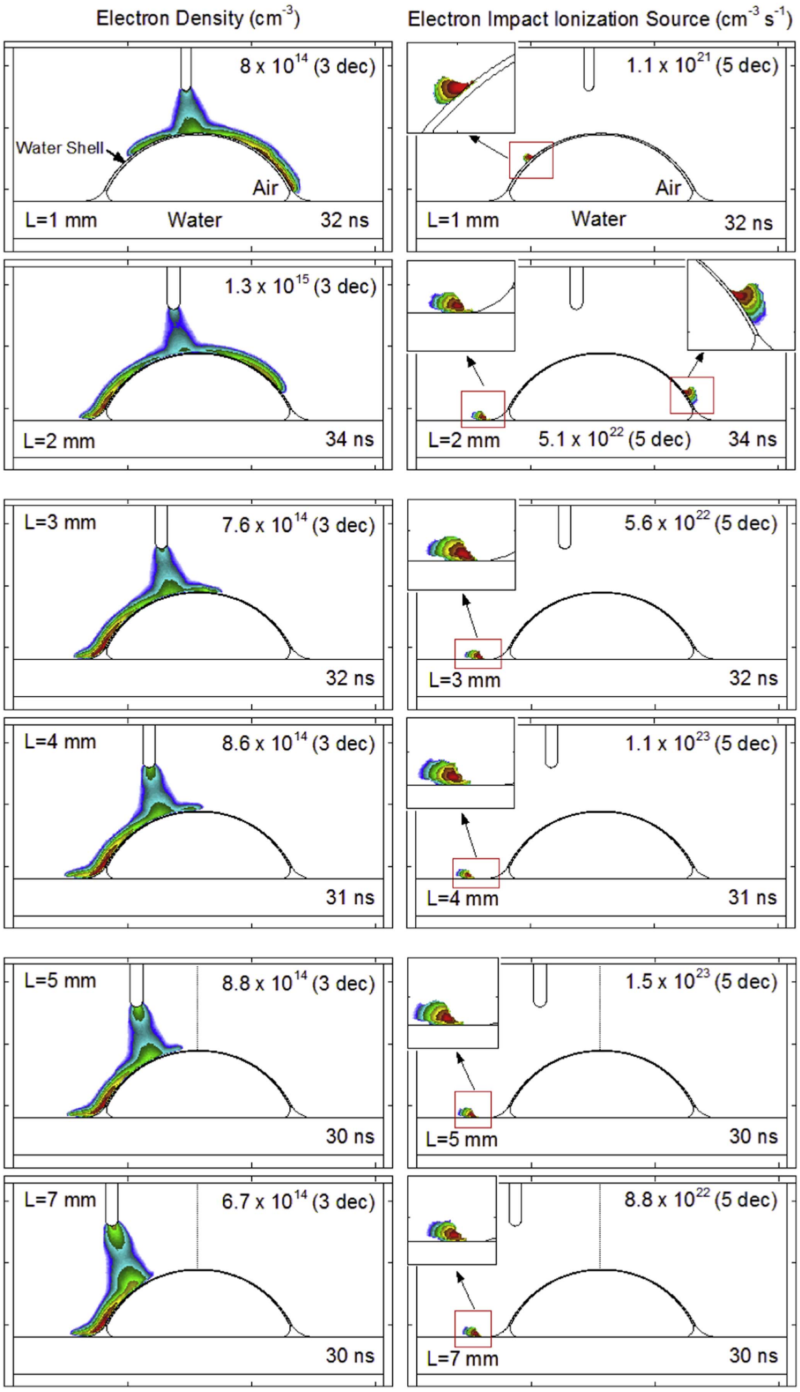

Figure 6. Electron density and electron impact ionization source for electrode offset $L = 1$, 2, 3, 4, 5 and 7 mm. The insets show enlargements of the surface ionization wave. The maximum value or range of values is shown for each frame.

However, with there being a finite conductivity of the shell, there is some tendency for the electric field to reorient to being perpendicular to the surface of the shell close to the surface. The lower vacuum electric field with increasing L produces slower avalanche speeds ($0.4 \times 10^8\,\mathrm{cm\,s^{-1}}$ for $L = 7$ mm and $0.25 \times 10^8\,\mathrm{cm\,s^{-1}}$ for $L = 10$ mm), and longer delays for the streamer to strike the bubble (25 ns for $L = 7$ mm and 40 ns for $L = 10$ mm).

As in the $L = 1$ mm case, after the volume streamer touches the shell, a SIW is launched. Due to the progressively larger component of the applied electric field pointing downward parallel to the surface, the SIW propagates only downhill for both $L = 7$ and 10 mm. The electron density and electron impact ionization source are shown in figure 6 for a selection of electrode offset values, $L = 1$–7 mm. The transition point at which propagation of the SIW is only *downhill* is $L = 6$–7 mm. For the smaller offset, the SIW propagates both uphill and downhill with gradually decreasing right (uphill) wing with increasing L.

The SIW extends the conductive plasma channel towards the edge of the bubble and, finally, to the grounded water layer. When the SIW reaches the flat water layer, a restrike

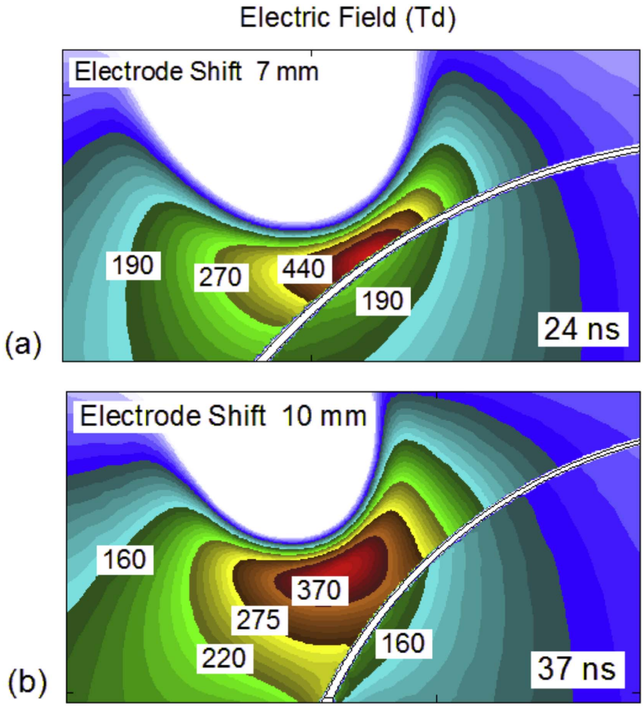

Figure 7. Electric field in vicinity of the streamer tip approaching the bubble surface for electrode offsets of (a) $L = 7$ mm and (b) $L = 10$ mm. Electric field enhancement occurs near the shell. At the same time, there is screening of the electric field from the interior of the shell by the conductive water-shell.

occurs back towards the powered electrode. The restrike takes the form of a negative ionization wave that propagates upwards through the surface hugging plasma on the shell, and through the plasma channel in the gas (see the last row of frames in figures 5(a) and (b)). The restrike occurs in part due to attachment and recombination in the plasma column during the 45 ns required for the SIW to reach the water layer. This reduction in electron density reduces the conductivity of the plasma column and enables a critically large electric field to be sustained to launch the restrike. Note that restrikes occur in most cases where the gap is large enough for attachment to occur and the electron density in the channel decays, a phenomenon that is also observed in plasma jets [36, 37].

Upon intersection of a streamer with the bubble-shell, a conductive streamer channel extends from the powered electrode to the surface of the shell, translating the applied potential to the bubble. Since the conductivity of the water shell is finite, there is only moderate electric field penetration through the shell to the interior of the bubble, as shown in figure 7. For example, for the offset $L = 7$ mm the electric field at the tip of the streamer exceeds 440 Td while that inside the bubble is not larger than 190 Td. For an offset of $L = 10$ mm the electric field outside the bubble is ≈400 Td whereas inside the bubble, the electric field is not larger than 160 Td. We found that the most sensitive parameter in determining the electric field inside the bubble was the

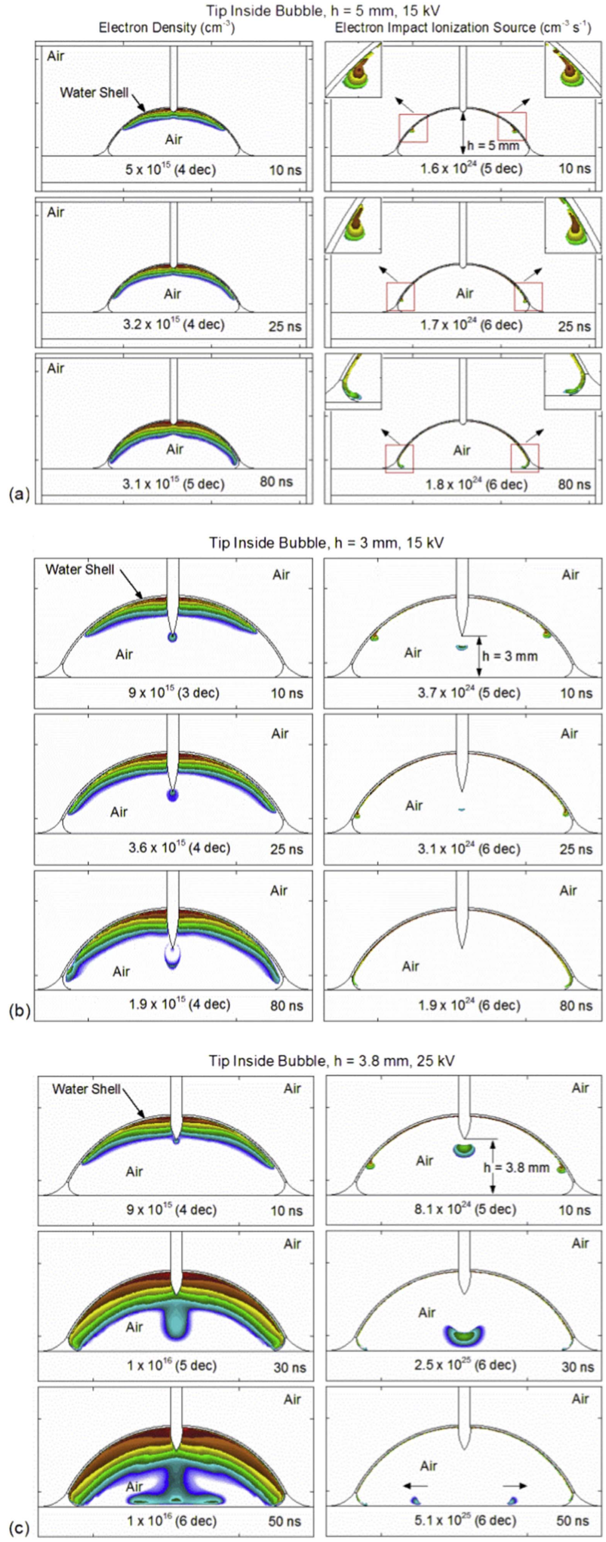

Figure 8. Plasma properties when the powered electrode tip is placed inside the water bubble-shell. (left) Electron density and (right) electron impact ionization source. (a) Electrode tip 5 mm above the water surface, $V = 15$ kV. The streamer propagates along the interior surface of the bubble, until reaching the water surface, at which time it propagates inwards. (b) Tip is 3 mm above the water, $V = 15$ kV. (c) Tip is 3.8 mm above the water surface, $V = 25$ kV. Both surface and volume streamers occur. The maximum value or range of values is shown for each frame.

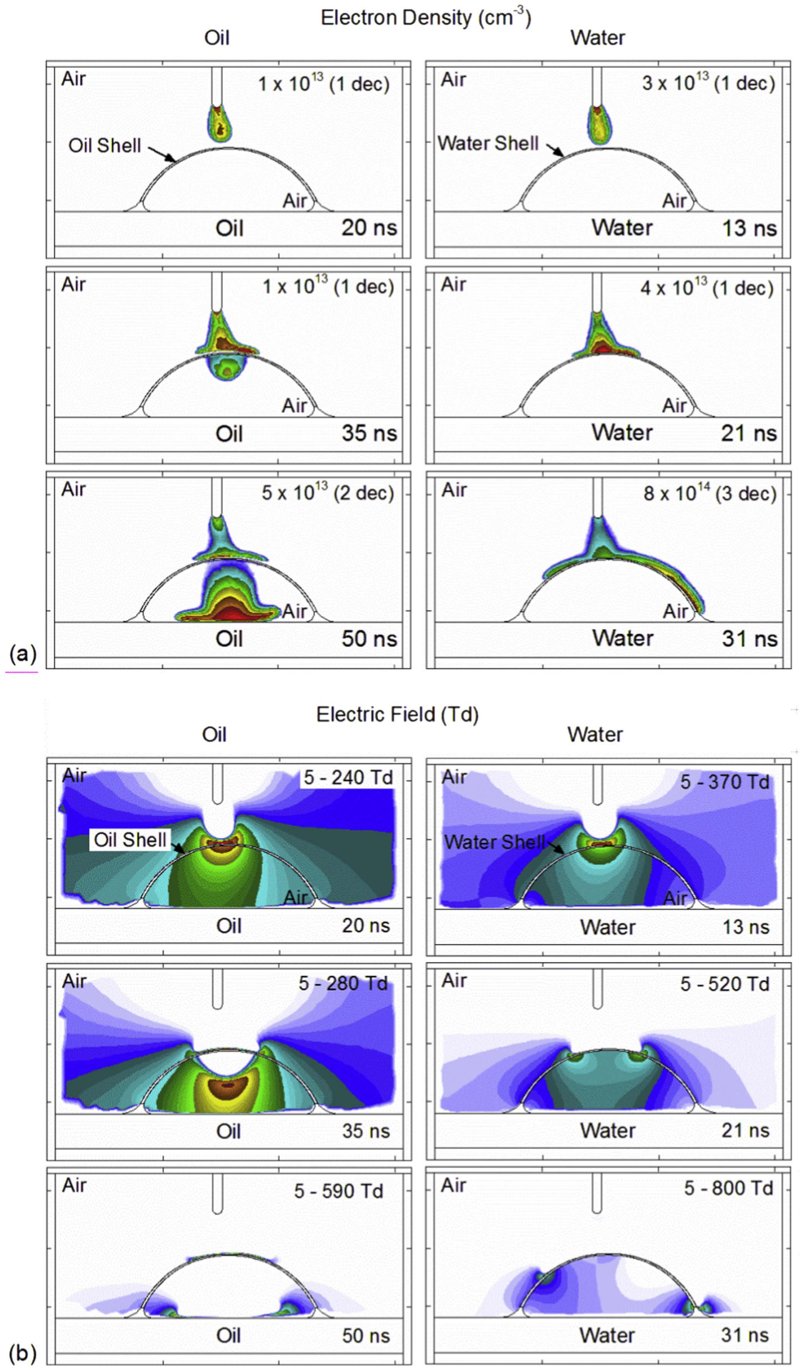

Figure 9. Time sequence of a streamer approaching and interacting with (left column) an oil bubble-shell and (right column) a water bubble-shell for $L = 1$ mm. (a) Electron density and (b) electric field. The streamer appears to penetrate through the oil bubble-shell (actually reinitiated) due to the low conductivity of its shell which allows the electric field to penetrate into the interior. The electric field is screened from the interior of the bubble by the conductive water-shell.

conductivity of the shell and (to a lesser extent) the dielectric constant of the shell.

When the electrode tip is inserted inside the bubble, the path of the streamer depends on how deeply the tip penetrates and on the applied voltage. With 15 kV applied to the tip and if the tip merely penetrates through the bubble with the tip near the inner surface, the streamer propagates along the inner surface of the top of the bubble. This trend, as also observed in the experiments [31], is shown in figure 8(a) where the tip is 5 mm above the surface of the water. In this case, the electric field enhancement that occurs at the surface of the shell produces a larger electric field parallel to the surface of the shell than the axial electric field directed towards the ground plane. The streamer is then generated as a SIW. Once launched, the SIW is self-sustained by the electric field at the streamer head. It stops propagating as soon as it touches the flat surface of the water (which has large capacitance and large conductivity). The electron density in the SIW inside the

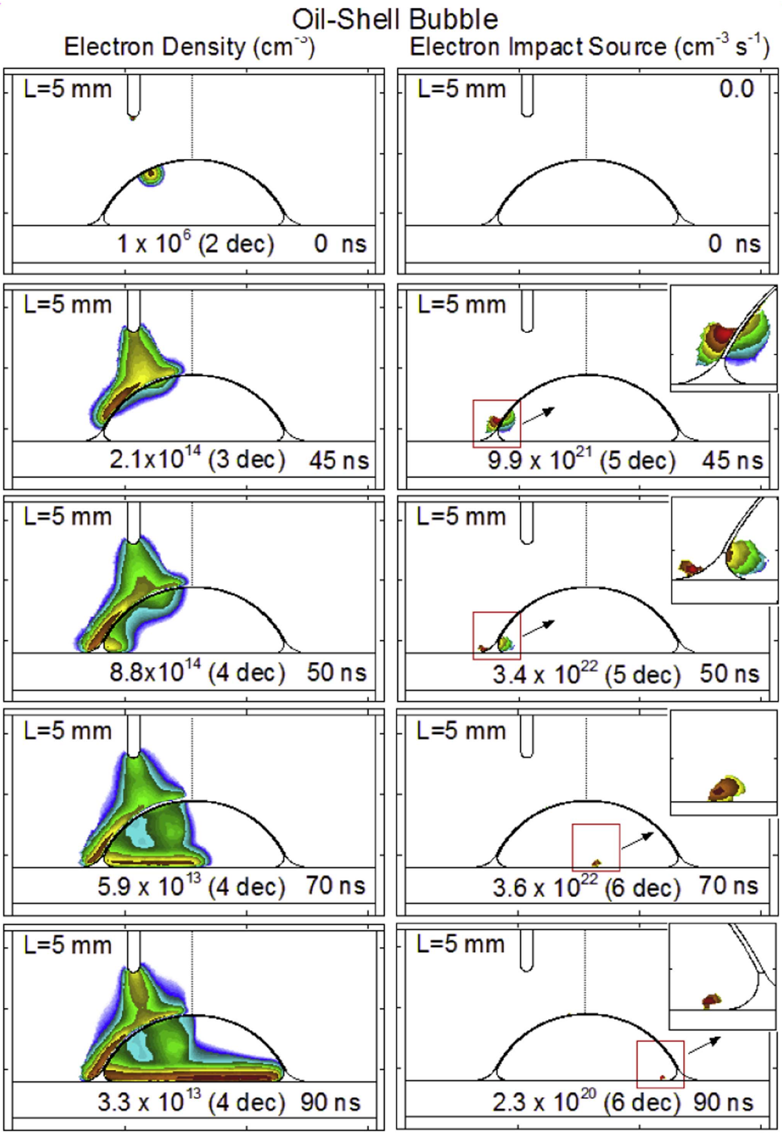

Figure 10. Plasma properties as a function of time for an oil-shell bubble with the electrode offset by $L = 5$ mm. (left) Electron density and (right) electron impact ionization source. The insets show enlargements of the surface ionization wave. The maximum value or range of values is shown for each frame.

bubble is $3 \times 10^{15}\,\mathrm{cm}^{-3}$, which is one-two decades larger than that for the SIW outside the bubble.

If the tip of the electrode penetrates deeply into the bubble two streamers can occur—a SIW and a weak volume streamer. These trends are shown in figure 8(b) for an applied potential of 15 kV and for the tip 3 mm above the surface of the water. The volume streamer decays before reaching the surface of the water, in part due to shielding of electric field by the evolving SIWs. With higher applied voltage (25 kV), the SIW and volume streamers can simultaneously propagate, shown in figure 8(c) for a tip height of 3.8 mm. The SIWs decay when they reach the flat water surface. Following touching the flat liquid, the volume streamer propagates as a counter-propagating SIW a short distance over the surface before decaying.

4. Streamer interaction with an oil bubble-shell

The behavior of positive streamers interacting with water bubble-shells is dominated in large part by the inability of the streamer to penetrate into the interior of the bubble due to the finite conductivity of the shell. Streamers behave quite differently when approaching a bubble-shell composed of non-conducting oil having a lower dielectric constant. With both the shell and underlying liquid being oil, the vacuum Laplacian electric field differs from that of the water shell. Comparisons of the electron density and electric field for streamers approaching oil and water bubble-shells are in figure 9 for $L = 1$ mm. Due to the lower conductivity and lower dielectric constant of the oil shell, the electric field lines experience little refraction and little electric field enhancement at the

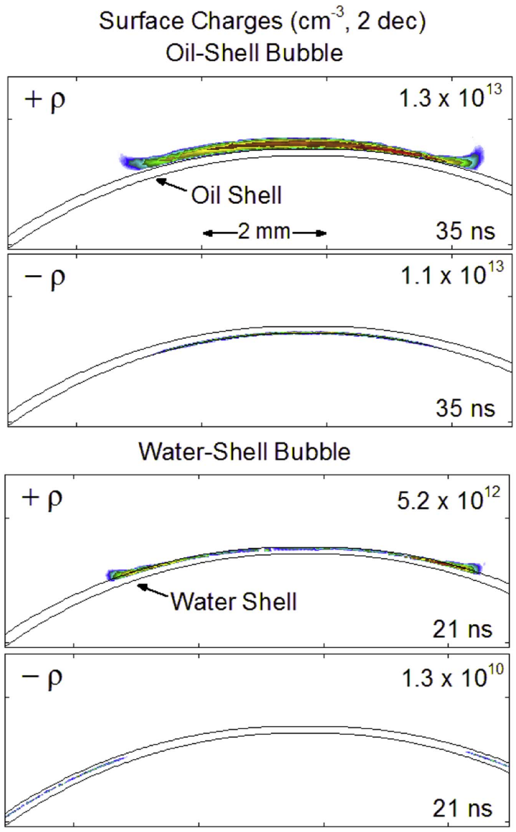

Figure 11. Comparison of the positive and negative space charges accumulated on oil and water bubble-shell. The amount of charge on the surface of the water bubble is three times lower than for the oil bubble.

surface of the shell. The approaching streamer rapidly charges the capacitance of the shell, producing an electric field of comparable magnitude inside the bubble as on the top of the bubble. With preionization in the bubble, this electric field is sufficient to reinitiate the streamer inside the bubble. With the relative absence of electric field enhancement at the inside surface of the bubble, a SIW is not launched, and the streamer propagates downward towards the ground plane.

This ability of streamers to be relaunched on the opposite side of dielectric layers has been previously investigated by simulations [38, 39] and experiments [40–42]. They found that re-ignition is ultimately due to penetration of electric field through the dielectric, with the re-ignition being sensitive to the dielectric constant, thickness, transparency (for ionizing radiation) and placement of the dielectric.

The re-initiation of a streamer inside an oil-shell bubble proceeds in a more complicated manner when the electrode tip is shifted from the bubble axis. As shown in figure 10 with $L = 5$ mm, following the initial volume streamer striking the shell, two SIWs are simultaneously initiated which propagate over the inner and outer surfaces of the shell. The component of the applied electric field parallel to the surface, both above and below the low conductivity shell, is large enough to support propagation of both SIW. After reaching the water surface, the SIW on the outer surface decays, while the SIW on the inner surface reverses direction and propagates across the surface of the liquid. There is sufficient surface charging (both inside and outside the bubble) that generates horizontal components of the electric field that the SIW can propagate along the surface of the water in the opposite direction from the vacuum field. As the SIW on the liquid passes under the tip, the propagation speed increases as now the vacuum electric field points in the direction of propagation. At about the time that the SIW reaches the bottom of the shell, a weak volume streamer inside the bubble is launched from the location at which the initial streamer strikes the outside of the bubble. This volume streamer crosses the shell and intersects the SIW on the liquid. The launching of this volume streamer is aided by vertical electric field components produced by charging of the bubble at the site of the initial streamer striking the bubble.

Due to the higher conductivity of water, the charge that accumulates on the outer and inner surfaces of the shell is dissipated during the finite dielectric relaxation time. At approximately the same time during the evolution of the discharge, the positive surface charge on the oil shell with a dielectric relaxation time of 1.2×10^{-6} s (1.3×10^{13} cm^{-3}) is nearly three times larger than that on the water shell (5×10^{12} cm^{-3}), as shown in figure 11. The re-initiation of the streamer inside the bubble produces charge on the interior surface of the shell as well [38, 39] showing positive charge accumulated on the outer shell and negative charges on the inner shell of the water and oil bubbles. The negative charges on the inner surface on the oil shell (1.1×10^{13} cm^{-3}) are nearly one order of magnitude larger in density than those on the water shell (1.3×10^{10} cm^{-3}).

5. Concluding remarks

The interaction of atmospheric pressure plasmas with foams has proven to be promising for producing high levels of activation in the liquid. Results from a two-dimensional computational investigation of a single streamer in air intersecting an isolated water or oil bubble-shell filled with humid air and floating on a liquid surface have produced insights to these processes. The conditions resemble those of recent experiments [31]. We found that, as in the experiments, a streamer striking a water bubble-shell pauses to charge the capacitance of the shell, and then propagates along the outside the shell as a SIW. The SIW will propagate both *uphill* (against the applied electric field) and *downhill* (with the applied electric field) depending on the location of the powered electrode. The conductivity of the tap-water shell is high enough to partly shield the applied field from the interior. Two consequences are that the incident streamer will align with the normal to the outer surface of the shell, and the electric field that penetrates into the bubble is too weak to reinitiate the streamer. Due to the low conductivity of the oil bubble-shell, the electric field significantly penetrates into the interior of the bubble. The streamer can then be re-initiated inside the bubble beneath the streamer. Note that the character of streamer interaction with a deionized (distilled) water bubble-shell, with a liquid conductivity one-two orders lower than that of tap water, can be expected to be similar to that of an oil bubble-shell.

Although the results discussed here are in qualitative agreement with experiments [31], the experiments were conducted on longer time scales (μs and ms) than the simulations. One phenomenon that is not captured in the simulations is perforation of the oil bubble-shell. This perforation takes place on millisecond time scales, and may be due to the mechanical stresses applied to the shell by differential charging on the top and bottom of the shell [28]. Analogous to the experiment, we also observed a streamer penetration into the oil bubble-shell. However, in the model, the penetration results from re-initiation of the streamer under the bubble-shell whereas in the experiment there is evidence that perforation of the shell enables the streamer to continue into the interior.

Acknowledgments

The work of NB and GN was supported by the Russian Science Foundation (Grant 14-12-01295-П). The work of MJK was supported by US Department of Energy Office of Fusion Energy Science (DE-SC000319 and DE-SC0014132), and the US National Science Foundation (PHY-1519117). The authors are grateful to Professor Yu Akishev for helpful discussions.

ORCID iDs

Natalia Yu Babaeva https://orcid.org/0000-0002-3762-8542
George V Naidis https://orcid.org/0000-0003-2184-802X
Mark J Kushner https://orcid.org/0000-0001-7437-8573

References

[1] Kolb J F, Joshi R P, Xiao S and Schoenbach K H 2008 Streamers in water and other dielectric liquids *J. Phys. D: Appl. Phys.* **41** 234007
[2] Levko D, Sharma A and Raja L L 2016 Microwave plasmas generated in bubbles immersed in liquids for hydrocarbons reforming *J. Phys. D: Appl. Phys.* **49** 22LT01
[3] Levko D, Sharma A and Raja L L 2017 Non-thermal plasma ethanol reforming in bubbles immersed in liquids *J. Phys. D: Appl. Phys.* **50** 085202
[4] Starikovskiy A, Yang Y, Cho Y I and Fridman A 2011 Nonequilibrium plasma in liquid water: dynamics of generation and quenching *Plasma Sources Sci. Technol.* **20** 024003
[5] Aoki H, Kitano K and Hamaguchi S 2008 Plasma generation inside externally supplied Ar bubbles in water *Plasma Sources Sci. Technol.* **17** 025006
[6] Gershman S, Mozgina O, Belkind A, Becker K and Kunhardt E 2007 Pulsed electrical discharge in bubbled water *Contrib. Plasma Phys.* **47** 19
[7] Bruggeman P, Leys C and Vierendeels J 2007 Experimental investigation of dc electrical breakdown of long vapour bubbles in capillaries *J. Phys. D: Appl. Phys.* **40** 1937
[8] Foster J E, Weatherford B R, Gillman E and Yee B 2010 Underwater operation of a DBD plasma jet *Plasma Sources Sci. Technol.* **19** 25001
[9] Vanraes P, Nikiforov A and Leys C 2012 Electrical and spectroscopic characterization of underwater plasma discharge inside rising gas bubbles *J. Phys. D: Appl. Phys.* **45** 245206
[10] Hamdan A and Cha M S 2015 Ignition modes of nanosecond discharge with bubbles in distilled water *J. Phys. D: Appl. Phys.* **48** 405206
[11] Tachibana K, Takekata Y, Mizumoto Y, Motomura H and Jinno M 2011 Analysis of a pulsed discharge within single bubbles in water under synchronized conditions *Plasma Sources Sci. Technol.* **20** 034005
[12] Sommers B S, Foster J E, Babaeva N Y and Kushner M J 2011 Observations of electric discharge streamer propagation and capillary oscillations on the surface of air bubbles in water *J. Phys. D: Appl. Phys.* **44** 082001
[13] Akishev Y S, Grushin M E, Karalnik V B, Petryakov A V and Trushkin N I 2012 Atmospheric pressure pulsed-periodical spark generator forming fast moving non-equilibrium plasma clouds *IEEE Trans. Plasma Sci.* **40** 2806–11
[14] Schmidt-Bleker A, Winter J, Iseni S, Dunnbier M, Weltmann K and Reuter S 2014 Reactive species output of a plasma jet with a shielding gas device—combination of FTIR absorption spectroscopy and gas phase modelling *J. Phys. D: Appl. Phys.* **47** 145201
[15] Van Gans W and Bogaerts A 2014 Reaction pathways of biomedically active species in an Ar plasma jet *Plasma Sources Sci. Technol.* **23** 035015
[16] Naidis G V 2014 Production of active species in cold helium–air plasma jets *Plasma Sources Sci. Technol.* **23** 065014
[17] Graves D B 2012 The emerging role of reactive oxygen and nitrogen species in redox biology and some implications for plasma applications to medicine and biology *J. Phys. D: Appl. Phys.* **45** 263001
[18] Kanazawa S, Kawano H, Watanabe S, Furuki T, Akamine S, Ichiki R, Ohkubo T, Kocik M and Mizeraczyk J 2011 Observation of OH radicals produced by pulsed discharges on the surface of a liquid *Plasma Sources Sci. Technol.* **20** 034010
[19] Bruggeman P and Leys C 2009 Non-thermal plasmas in and in contact with liquids *J. Phys. D: Appl. Phys.* **42** 053001
[20] Bruggeman P J *et al* 2016 Plasma–liquid interactions: a review and roadmap *Plasma Sources Sci. Technol.* **25** 053002
[21] Adamovich I *et al* 2017 The 2017 plasma roadmap: low temperature plasma science and technology *J. Phys. D: Appl. Phys.* **50** 323001
[22] Foster J E 2017 Plasma-based water purification: challenges and prospects for the future *Phys. Plasmas* **24** 055501
[23] Vardar-Sukan F 1998 Foaming: consequences, prevention and destruction *Biotechnol. Adv.* **16** 913–48
[24] Rafati A M and Ashrafizadeh S N 2010 The importance of foams and antifoaming in bioprocesses *Pak. J. Biotechnol.* **7** 19–39
[25] Schugerl K 2000 Recovery of proteins and microorganisms from cultivation media by foam flotation *Advances in Biochemical Engineering/Biotechnology* ed T Scheper vol 68 (Berlin: Springer)
[26] Carr E L, Eales K, Soddell J and Seviour R J 2005 Improved permeabilization protocols for fluorescence *in situ* hybridization (FISH) of mycolic-acid containing bacteria found in foams *J. Microbiol. Methods* **61** 47–54
[27] Chisti Y 1993 Animal cell culture in stirred bioreactors: observations on scale-up *Process Biochem.* **28** 511–7

[28] Bird J C, de Ruiter R, Courbin L and Stone H A 2010 Daughter bubble cascades produced by folding of ruptured thin films *Nature* **465** 759
[29] Izmailov M M, Kazenin D A, Kutepov A M and Tsablinova I A 1990 Methods and equipment for foam damping using electric and magnetic effects *Chem. Petrol. Eng.* **26** 463
[30] Shidong Y, Fengguo C and Jun M 2008 Preliminary study on control of water treatment foam by pulsed high voltage discharge *2nd Int. Conf. on Bioinformatics and Biomedical Engineering, ICBBE*
[31] Akishev Y, Arefi-Khonsari F, Demir A, Grushin M, Karalnik V, Petryakov A and Trushkin N 2015 The interaction of positive streamers with bubbles floating on a liquid surface *Plasma Sources Sci. Technol.* **24** 065021
[32] Norberg S A, Johnsen E and Kushner M J 2015 Formation of reactive oxygen and nitrogen species by repetitive negatively pulsed helium atmospheric pressure plasma jets propagating into humid air *Plasma Sources Sci. Technol.* **24** 035026
[33] Babaeva N Y, Tereshonok D V and Naidis G V 2016 Fluid and hybrid modelling of nanosecond surface discharges: effect of polarity and secondary electrons emission *Plasma Sources Sci. Technol.* **25** 044008
[34] Babaeva N Y and Kushner M J 2013 Reactive fluxes delivered by dielectric barrier discharge filaments to slightly wounded skin *J. Phys. D: Appl. Phys.* **46** 025401
[35] Loeb L B 1959 Significance of formative time lags in gaseous breakdown *Phys. Rev.* **113** 7
[36] Sigmond R S 1984 The residual streamer channel: return stroke and secondary streamer *J. Appl. Phys.* **56** 1355
[37] Darny T, Pouvesle J-M, Peuch V, Douat C, Dozias S and Robert E 2017 Analysis of conductive target influence in plasma jet experiments through helium metastable and electric field measurements *Plasma Source Sci. Technol.* **26** 045008
[38] Pechereau F, Jansky J and Bourdon A 2012 Simulation of the reignition of a discharge behind a dielectric layer in air at atmospheric pressure *Plasma Sources Sci. Technol.* **21** 055011
[39] Pechereau F and Bourdon A 2014 Influence of the polarity of the applied voltage on the reignition of a discharge below a dielectric layer in air at atmospheric pressure *J. Phys. D: Appl. Phys.* **47** 445206
[40] Algwari Q T and O'Connell D 2011 Plasma jet interaction with a dielectric surface *IEEE Trans. Plasma Sci.* **39** 2368–9
[41] Lu X *et al* 2009 Propagation of an atmospheric pressure plasma plume *J. Appl. Phys.* **105** 043304
[42] Wu S, Wang Z, Huang Q, Xiong Q and Lu X 2011 Plasma plume ignited by plasma plume at atmospheric pressure *IEEE Trans. Plasma Sci.* **39** 2292–3